

This work was written as part of one of the author's official duties as an Employee of the United States Government and is therefore a work of the United States Government. In accordance with 17 U.S.C. 105, no copyright protection is available for such works under U.S. Law.

Public Domain Mark 1.0

<https://creativecommons.org/publicdomain/mark/1.0/>

Access to this work was provided by the University of Maryland, Baltimore County (UMBC) ScholarWorks@UMBC digital repository on the Maryland Shared Open Access (MD-SOAR) platform.

Please provide feedback

Please support the ScholarWorks@UMBC repository by emailing scholarworks-group@umbc.edu and telling us what having access to this work means to you and why it's important to you. Thank you.

RESEARCH ARTICLE

10.1002/2015JD023878

Key Points:

- Significant calibration updates from MODIS Terra C5 to C6
- Calibration updates improve the MODIS Deep Blue AOD retrieval
- The Terra C6 Deep Blue AOD data set is stable over the mission to date

Correspondence to:

A. M. Sayer,
andrew.sayer@nasa.gov

Citation:

Sayer, A. M., N. C. Hsu, C. Bettenhausen, M.-J. Jeong, and G. Meister (2015), Effect of MODIS Terra radiometric calibration improvements on Collection 6 Deep Blue aerosol products: Validation and Terra/Aqua consistency, *J. Geophys. Res. Atmos.*, 120, 12,157–12,174, doi:10.1002/2015JD023878.

Received 30 JUN 2015

Accepted 11 NOV 2015

Accepted article online 13 NOV 2015

Published online 14 DEC 2015

Effect of MODIS Terra radiometric calibration improvements on Collection 6 Deep Blue aerosol products: Validation and Terra/Aqua consistency

A. M. Sayer^{1,2}, N. C. Hsu¹, C. Bettenhausen^{1,3}, M.-J. Jeong⁴, and G. Meister¹

¹NASA Goddard Space Flight Center, Greenbelt, Maryland, USA, ²Goddard Earth Sciences Technology and Research (GESTAR), Universities Space Research Association, Greenbelt, Maryland, USA, ³Science Systems and Applications, Inc., Lanham, Maryland, USA, ⁴Gangneung-Wonju National University, Gangneung City, Korea

Abstract The Deep Blue (DB) algorithm's primary data product is midvisible aerosol optical depth (AOD). DB applied to Moderate Resolution Imaging Spectroradiometer (MODIS) measurements provides a data record since early 2000 for MODIS Terra and mid-2002 for MODIS Aqua. In the previous data version (Collection 5, C5), DB production from Terra was halted in 2007 due to sensor degradation; the new Collection 6 (C6) has both improved science algorithms and sensor radiometric calibration. This includes additional calibration corrections developed by the Ocean Biology Processing Group to address MODIS Terra's gain, polarization sensitivity, and detector response versus scan angle, meaning DB can now be applied to the whole Terra record. Through validation with Aerosol Robotic Network (AERONET) data, it is shown that the C6 DB Terra AOD quality is stable throughout the mission to date. Compared to the C5 calibration, in recent years the RMS error compared to AERONET is smaller by ~ 0.04 over bright (e.g., desert) and ~ 0.01 – 0.02 over darker (e.g., vegetated) land surfaces, and the fraction of points in agreement with AERONET within expected retrieval uncertainty higher by $\sim 10\%$ and $\sim 5\%$, respectively. Comparisons to the Aqua C6 time series reveal a high level of correspondence between the two MODIS DB data records, with a small positive (Terra-Aqua) average AOD offset < 0.01 . The analysis demonstrates both the efficacy of the new radiometric calibration efforts and that the C6 MODIS Terra DB AOD data remain stable (to better than 0.01 AOD) throughout the mission to date, suitable for quantitative scientific analyses.

1. Introduction

The two spaceborne Moderate Resolution Imaging Spectroradiometers (MODIS) have been used extensively for quantitative Earth science applications, including the study of atmospheric aerosols. NASA's routine MODIS data processing includes algorithms dedicated to midvisible aerosol optical depth (AOD) retrieval [Hsu *et al.*, 2004; Levy *et al.*, 2013], as well as others which provide AOD as a by-product of atmospheric correction for determination of land or ocean surface reflectance [e.g., Ahmad *et al.*, 2010; Lyapustin *et al.*, 2011]. MODIS has been providing data since early 2000 aboard the Terra platform and mid-2002 on the Aqua platform, with daytime Equatorial local solar crossing times of 10:30 and 13:30, respectively, and both sensors are presently operating well past their 6 year design lives. The MODIS data records are reprocessed periodically with temporally consistent algorithms and radiometric calibration; the most recent reprocessing (Collection 6, C6) of Atmosphere discipline data products was released beginning early 2014 and is complete for both sensors, with forward processing ongoing. These supersede the previous Collections 5 and 5.1 (hereafter C5) products.

Deep Blue (DB) is one such aerosol data product, developed initially [Hsu *et al.*, 2004] to provide coverage over bright surfaces (such as deserts) which were not covered by the MODIS Dark Target (DT) aerosol data set due to surface reflectance assumptions in the DT algorithm [Kaufman *et al.*, 1997; Levy *et al.*, 2013]. With C6, an enhanced DB algorithm was developed, extending spatial coverage to include these dark (vegetated) land surfaces in addition to bright surfaces [Hsu *et al.*, 2013] and improving the quality of the retrieved AOD compared to C5 [Sayer *et al.*, 2013]. The enhanced DB algorithm has also been applied to the (1997–2010) Sea-viewing Wide Field-of-view Sensor (SeaWiFS) data record [Hsu *et al.*, 2012; Sayer *et al.*, 2012a], and a version is in development for the Visible Infrared Imaging Radiometer Suite (VIIRS), launched late 2011; the SeaWiFS and VIIRS applications also include a separate over-water algorithm [Sayer *et al.*, 2012b] to complement

the over-land DB data, while in MODIS water pixels are processed by the DT ocean algorithm. This study is concerned with the MODIS application of DB, i.e., only retrievals over land surfaces.

The key MODIS bands used by the DB land algorithm are 8, 3, and 1, centered near 412, 470, and 650 nm, respectively. The main data product is the AOD at 550 nm. Throughout this study references to AOD indicate the AOD at 550 nm, unless indicated otherwise. The DB algorithm has two processing paths to determine which bands are used in the retrieval and how the spectral surface reflectance is estimated, while aerosol optical models are set based on region and season [Hsu *et al.*, 2013]. Internal checks based on surface and top of atmosphere (TOA) brightness are used to determine whether a given pixel is processed with the “arid” path, which uses bands 8 and 3 (and band 1 in cases of heavy dust), or the “vegetated” path, which uses bands 3 and 1. Note that the terms arid and vegetated are often used as shorthand for simplicity, as bright scenes often correspond to arid regions and dark scenes to vegetated regions, although these are descriptive terms only. So-called arid surfaces, for example, can include not only sandy deserts but also rocky surfaces, bare or sparsely vegetated soil, and urban areas.

As the older of the two sensors, MODIS Terra has degraded to a greater extent than MODIS Aqua, requiring additional efforts by the MODIS Characterization Support Team (MCST) and Ocean Biology Processing Group (OBPG) to maintain and improve the radiometric quality of the instrument. As such C6 Aqua data were released before Terra data, and previous studies of the C6 aerosol products [Hsu *et al.*, 2013; Levy *et al.*, 2013; Munchak *et al.*, 2013, Munchak *et al.*, 2013; Remer *et al.*, 2013; Sayer *et al.*, 2013, 2014; Sorek-Hamer *et al.*, 2015] have focused largely on Aqua. MODIS Terra’s degradation has also been more rapid because of an anomaly with the solar diffuser door in 2003, leading to it remaining open [Erives *et al.*, 2004]. Although calibration corrections were developed by MCST and OBPG and applied in C5 DB processing, band 8 degradation was sufficiently severe that forward processing of DB for MODIS Terra was stopped at the end of 2007 [Jeong *et al.*, 2011] as adequate corrections had not been developed at that time. The time span of the corrections has been extended for C6, such that DB forward processing for both Terra and Aqua is expected to continue for the foreseeable future.

The purpose of this study is to describe and evaluate the effect of radiometric calibration improvements on the Terra C6 DB record through comparison against Aerosol Robotic Network (AERONET) [Holben *et al.*, 1998] data and examine the consistency between Terra and Aqua DB data. Algorithmic updates from C5 to C6 and their effects on validation were discussed and quantified by Hsu *et al.* [2013] and Sayer *et al.* [2013]. This study is organized as follows: Section 2 describes MODIS and radiometric calibration updates from C5 to C6, and section 3 evaluates the effect of these improvements on the DB data via AOD evaluation against AERONET. Section 4 examines consistency between the Terra and Aqua DB records, and section 5 provide a summary and perspective.

2. The MODIS Sensor and Radiometric Calibration Improvements

2.1. MODIS Overview

MODIS takes measurements in a total of 36 reflective solar and thermal emissive bands (RSB and TEB, respectively), with a nominal pixel size between 250 m and 1 km (dependent on band). The DB algorithm uses these level 1b (L1b, calibrated radiance) data aggregated to 1 km and provides level 2 (L2, geophysical products), in this case AOD, by performing retrievals on the 1 km data and then aggregating to nominal 10 km pixel size [Hsu *et al.*, 2013]. Note that DB uses only pixels identified as land surfaces by the MODIS internal land mask (at 1 km resolution).

Both level 1 and level 2 products are organized in granules, which consist (for 1 km data) of 1354 pixels across track and 2030 along track, representing 5 min of data collection. The sensor scans across track back and forth, recording 10 of these 1 km pixels each time. Thus, a granule consists of 203 scans. The light observed by MODIS is reflected from a scan mirror onto the focal plane assemblies; as the sensor scans back and forth, both sides of this scan mirror are used. Differences in the quality of the characterization of these two mirror sides can lead to striping in the data between forward and reverse scans in some situations [Franz *et al.*, 2007a]. Because of the scan geometry, the spatial resolution degrades from nadir to the scan edge (i.e. pixels near the edge of the scan are larger than those near nadir); the resulting swath width is ~2330 km. Additionally, this scan geometry results in overlap between pixels from consecutive scans near the swath edges (the “bowtie effect”).

The MCST calibration analyses are used to create the standard MODIS L1b products, used for routine MODIS processing by most of the science team algorithms. Toller *et al.* [2013] describe the algorithm used by MCST

to create the calibrated L1b products from MODIS measurements for C6. The same basic methodology was applied to previous Collections as well. However, as knowledge of MODIS' in-flight characterization improves through time, MCST L1b data from C5 and C6 differ. In brief, each pixel's calibration depends on band, detector, mirror side, and time. In addition to prelaunch characterization [Barnes *et al.*, 1998], MODIS RSBs are calibrated routinely using an onboard solar diffuser (SD) and SD stability monitor, with additional information from periodic lunar observations [e.g., *Erives et al.*, 2004; *Sun et al.*, 2007; *Xiong et al.*, 2007; *Wu et al.*, 2013]. These on board and vicarious techniques are used to monitor RSB absolute calibration and stability, and used to develop and apply calibration corrections where needed, with a target RSB accuracy of order 2% in reflectance under typical conditions [Toller *et al.*, 2013].

Due to the small contribution of subsurface ocean constituents to the TOA reflectance in the visible spectral range, ocean color analyses have very strict radiometric requirements of order 1% accuracy and 0.5% decadal stability [e.g., *Gordon*, 1988; *McClain et al.*, 2004]. The OBPG found that the MCST calibration of some MODIS Terra bands was insufficient for this [Franz *et al.*, 2007a] and so developed vicarious calibration corrections for the relevant bands; specifically, a correction for the polarization sensitivity of the sensor, which includes adjustments to the detector response versus scan angle and gain [Meister *et al.*, 2005, 2011, 2014; Franz *et al.*, 2007b; Kwiatkowska *et al.*, 2008]. In ocean color processing, these OBPG vicarious calibration corrections are applied as an additional factor on top of (not instead of) the standard MCST L1b data. An older version of these OBPG corrections was applied to the C5 DB Terra record [Jeong *et al.*, 2011]. In C6 DB, OBPG corrections are applied to bands 8 and 3 (412 and 470 nm). This strategy is conceptually similar to, although a different implementation from, the so-called "C6+" calibration analysis of Lyapustin *et al.* [2014]. A summary of these corrections is provided below, although the reader is directed to the above references for full details. In recent years OBPG also apply a gain correction for certain MODIS Aqua bands, although a polarization sensitivity correction has not yet been necessary [Meister *et al.*, 2012].

2.2. OBPG Vicarious Calibration

The OBPG radiance correction takes the form

$$L_m = M_{11}L_t + M_{12}(Q_t \cos 2\alpha + U_t \sin 2\alpha) + M_{13}(-Q_t \sin 2\alpha + U_t \cos 2\alpha) + M_{14}V_t \quad (1)$$

where (L_t, Q_t, U_t, V_t) is the Stokes vector (with L_t the true radiance, which is the parameter of interest), L_m the measured radiance, M_{11} to M_{14} the elements of the first line of the Mueller matrix (describing the sensitivity of the sensor to polarization of incident light), and α the angle of rotation between the instrument and atmospheric reference frames. The parameter M_{11} represents a gain correction [Franz *et al.*, 2007b], M_{12} and M_{13} the sensitivity to linearly polarized light, determined prelaunch [Sun and Xiong, 2007] but with a trending coefficient determined by the OBPG analysis, and M_{14} the sensitivity to circularly polarized light, which is neglected as $V_t \approx 0$ at TOA.

The gain correction M_{11} is applied first, and polarization sensitivity corrections are then normalized to give $m_{12} = M_{12}/M_{11}$, $m_{13} = M_{13}/M_{11}$. Thus, equation (1) can be simplified to

$$L_t = L_m/M_{11} - m_{12}(Q_t \cos 2\alpha + U_t \sin 2\alpha) - m_{13}(-Q_t \sin 2\alpha + U_t \cos 2\alpha). \quad (2)$$

The required instrument characterization parameters M_{11} , m_{12} , m_{13} are provided by OBPG as a function of scan angle, mirror side, detector, and time. These are detailed most recently by Meister *et al.* [2014], and at present MODIS Aqua ocean color products are used as the data source for vicarious calibration. Lookup tables of (Q_t, U_t) are created from radiative transfer simulations as a function of solar/view geometry and surface reflectance. Note that these lookup tables assume that aerosol has no TOA polarization signal; the residual error from this assumption is, in most cases, negligible [Meister *et al.*, 2014]. These are applied via equation (2) as additional correction factors to the MCST L1b data in DB processing. DB works in reflectance units; i.e., the radiances are normalized by the solar constant after these corrections are applied.

2.3. Calibration Effect on TOA Reflectance and Retrieved AOD

In the following analyses, three different L1b calibration data sets are used: "C6," corresponding to the operational C6 DB processing (i.e., MCST C6 L1b with additional OBPG corrections to bands 3 and 8), "C6-" (MCST C6 L1b without OBPG corrections), and "C5" (MCST C5 L1b, again without OBPG corrections). In all cases the current operational DB algorithm is used [Hsu *et al.*, 2013]; the only difference between the runs is in the

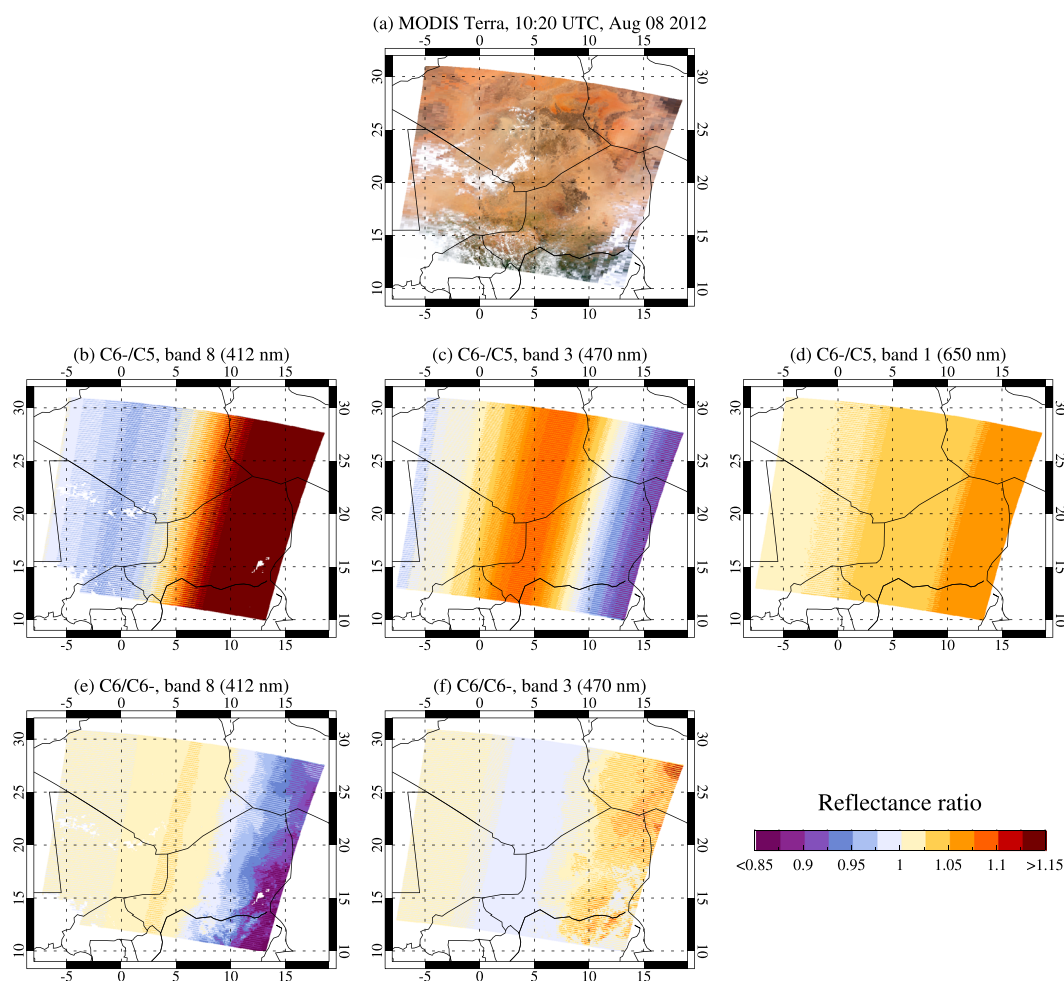


Figure 1. Magnitude of calibration corrections for an example MODIS Terra granule. (a) A true color image and (b–d) the ratio between C6- and C5 calibrations at each of bands 8, 3, and 1 (412, 470, 650nm), respectively. (e and f) The corresponding ratio between C6 and C6-. Note some portions of 412nm images are missing due to detector saturation.

L1b calibration applied. This enables a direct evaluation of the effect of calibration changes on the DB AOD retrieval. Note that the Dark Target land and ocean data products [Levy *et al.*, 2013] do not apply these OBPG corrections at present but do use the latest MCST L1b data which is equivalent to the C6- run in this study.

An example granule over northern Africa from the year 2012 is shown in Figure 1. For this particular granule, applying the MCST updates from C5 to C6- results in reflectance changes of up to more than 15% for band 8 (412 nm) and somewhat less for bands 3 (470 nm) and 1 (650 nm). The geometric dependence of the corrections is evident, as is the striping in the corrections, resulting from different corrections to each of the two scan mirror sides. The additional OBPG corrections (going from C6- to C6+ as applied in DB processing) are smaller in comparison; they are in some cases the same sign and in other cases of opposite sign to the changes made between the C5 and C6- runs. Note that no OBPG correction is applied to band 1 (650 nm); no additional correction to the MCST L1bs was necessary, due to limited polarization sensitivity of the band and limited evidence for uncorrected degradation in the MCST product. However, the MCST calibration for this band was updated between the C5 and C6-/C6+ runs.

Figure 2 shows TOA reflectance near the eastern edge of the swath. A “sawtooth” pattern is evident in the C5 and C6- data, particularly at 412 nm. This is the result of inaccuracies in the calibration coefficients applied to one or both of the scan mirror sides and results in striping of the TOA reflectance images. With the OBPG corrections applied (C6 run), this striping is greatly reduced.

The effect of these calibration updates on retrieved AOD is shown in Figure 3 for this same granule. The C6 AOD shows hotspots where dust storms are visible in Figure 1, with peak AOD exceeding 2 in the

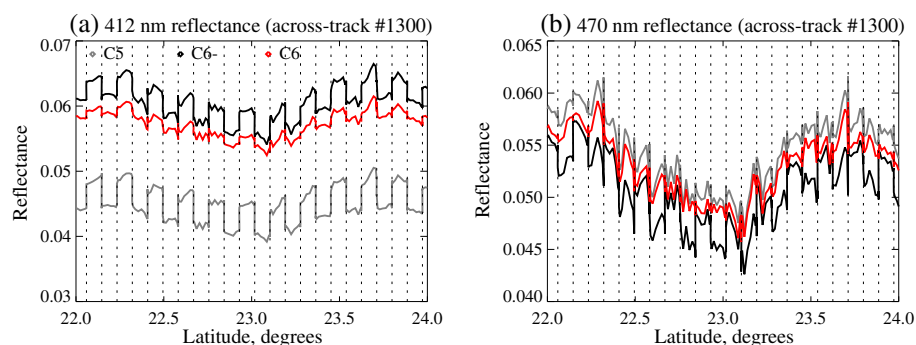


Figure 2. TOA reflectance at 412 and 470 nm for a section (across-track position 1,300 of 1,354) of the granule shown in Figure 1. Vertical dashed lines indicate the first detector in each scan. C5 L1b data are shown in gray, C6- in black, and C6 in red.

thickest plumes. Striping in the AOD retrieval is minor, consistent with the reduction of striping shown in Figure 2 in the C6 run. The changes in retrieved AOD going from C6 to C6-, and from C6- to C5, show strong geometric and mirror side dependence (i.e., they are striped). The large magnitudes of the changes in AOD, which can exceed 0.5 in places, illustrates that the potential effects on the MODIS DB AOD record of sensor radiometric calibration problems can be severe.

3. Evaluation Against AERONET AOD

3.1. AERONET Data and Matchup Protocol

The sun photometers used by AERONET observe direct solar radiation and, through correction for scattering and absorption by atmospheric gases, derive total columnar spectral AOD with uncertainty ~ 0.01 in the mid-visible [Holben et al., 1998; Eck et al., 1999]. The standard configuration of these instruments provides AOD at 440, 675, 870, and 1020 nm; some sensors have filters for additional wavelengths. Under cloud-free conditions, observations are taken every ~ 15 min. The AERONET level 2 data product, recommended for quantitative use, has undergone automatic cloud screening [Smirnov et al., 2000], manual inspection, and recalibration against reference AERONET photometers (which are maintained with higher calibration accuracy than sensors in the field). This data product is used here; as AERONET level 2 processing typically runs several months to years behind real time (due in part to the need for the instruments to be returned for recalibration), the analysis is performed using AERONET data from 2000 to 2014.

Due to the high data quality and standardized protocols across a global range of sites, AERONET offers the most practical means for the large-scale validation of satellite AOD data sets. In this study, as the purpose is to assess calibration stability and its effects on AOD, a total of 22 AERONET sites with long time series are used. Although there are hundreds of sites providing AERONET data, only a small number provide complete or

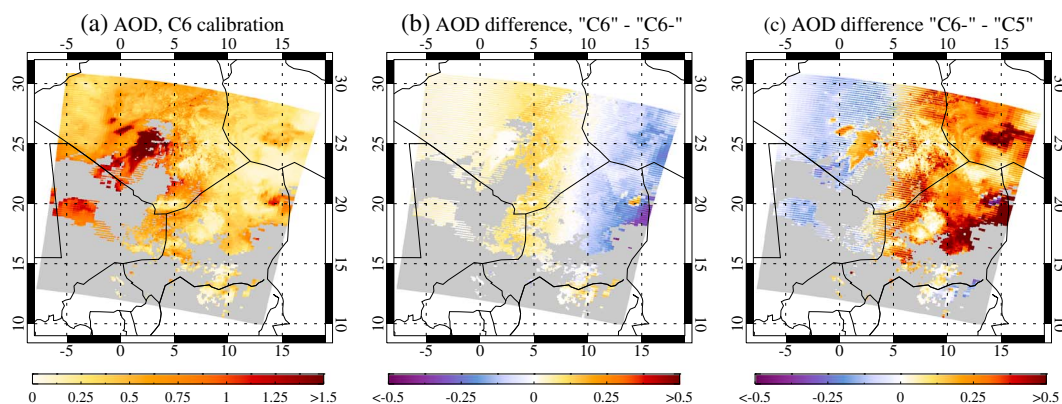


Figure 3. Effect of calibration changes on DB AOD retrieval for the granule shown in Figure 1. (a) The retrieved AOD for the C6 run, (b) the difference between C6 and C6- runs, and (c) the difference between C6- and C5 runs. Pixels without retrievals, due to e.g., cloud cover, are shown in gray.

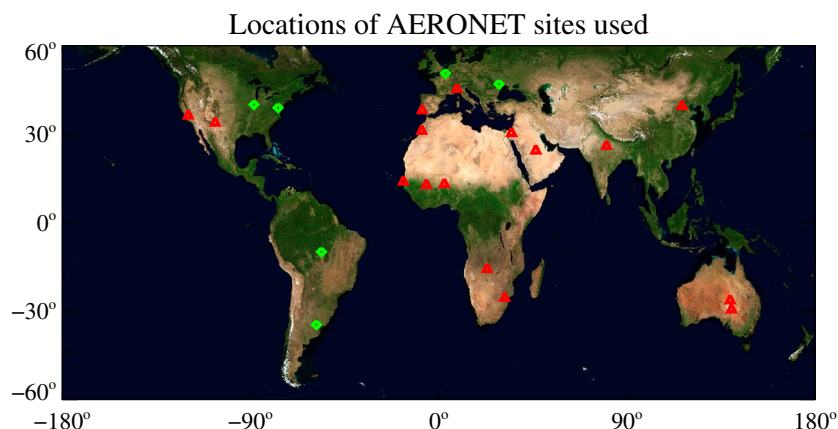


Figure 4. Locations of the 22 long-term AERONET sites used in this study. Green diamonds show sites processed using the vegetated DB path and red triangles the arid DB path.

near-complete data over the bulk of the Terra record (2000 to present). Thus, there is a compromise between the total data volume available and the ability to ensure a reasonably consistent grouping of sites, each with their own surface/atmospheric characteristics, from one year to the next. Large changes in the sampling of AERONET sites used might otherwise affect the apparent stability of the validation.

The locations of these sites are shown in Figure 4. Six (Table 2) are in locations where the vegetated DB algorithm path is applied and thus are sensitive to calibration changes in bands 1 and 3 but unaffected by changes to band 8, while 16 (Table 3) are in locations where the arid path is applied and thus are sensitive to changes in bands 3 and 8 (cf. section 1 and Hsu *et al.* [2013]). For the present analysis, MODIS granules for these sites have been processed applying the C6 DB AOD retrieval algorithm to each of the three (C5, C6-, and C6) L1b data sets.

AERONET provides repeated point measurements of the aerosol column between the ground and the Sun, while satellites provide a snapshot of the aerosol column between ground and sensor, across a swath. Thus, there are spatiotemporal sampling differences between the two. To mitigate the effects of these sampling differences, this study adopts a spatiotemporal averaging method of the type first applied on a global scale by Ichoku *et al.* [2002] (since modified and used by many others). Specifically, AERONET data are averaged within ± 30 min of the Terra overpass time and DB data within ± 25 km of the AERONET site. As the main focus of this study is the change in statistics between the three calibration runs, the importance of the exact matchup protocol is secondary. Internal checks assign each DB pixel a quality assurance (QA) value ranging from 1 (poor) to 3 (best); only pixels with $QA \geq 2$ are used here, which is the general recommendation for quantitative use of DB data [Hsu *et al.*, 2013; Sayer *et al.*, 2013].

The AERONET AOD at 550 nm is denoted as τ_A and is obtained by interpolating the spectrally closest AERONET AOD (normally 440 or 500 nm) using the standard Ångström exponent α provided within the AERONET data. A valid matchup is defined when there is at least one valid MODIS retrieval near the site and at least one AERONET observation near the time of the satellite overpass.

Additionally, it is required that there are MODIS retrievals for each of the three L1b calibration runs (C5, C6-, and C6), in order to ensure that the population of AERONET data sampled is the same for each. In practice, this additional constraint removes 1–5% of matchups, dependent on site. The differences in retrieval availability between runs arise because the changing calibration affects cloud masking and QA tests. Changes of a few percent in TOA reflectance can cause some pixels to pass or fail some of the threshold-based cloud masking tests [Hsu *et al.*, 2013] differently between the runs. This mostly happens near cloud edges, resulting in a change of the number of cloud-free sensor pixels identified within the retrieval box, which is one of the factors used to assign retrieval QA. As reflectance can either increase or decrease as a result of calibration updates, the difference between different calibrations does not lead to a systematic increase or decrease in the number of pixels identified as cloudy between the three runs.

A total of 36,830 matches are obtained over the 22 sites. Their temporal distribution is shown in Figure 5; the data volume is markedly lower in 2014 as AERONET data from some sites are not yet available at level 2 and

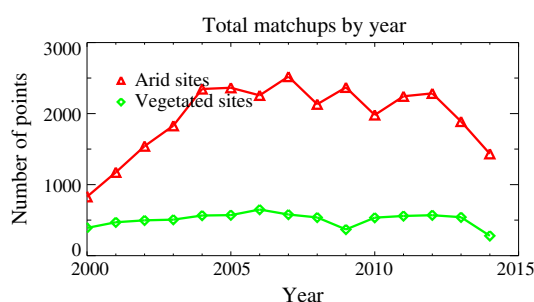


Figure 5. Number of matchups between MODIS Terra DB and AERONET at vegetated (green diamond) and arid (red triangle) sites.

expected to approximate a Gaussian distribution with mean zero and variance 1. Thus, compared to a reference truth, one standard deviation ($\sim 68\%$) of data points should match to within $\pm EE$, two standard deviations ($\sim 95\%$) within twice this EE, and so forth.

Based on validation against 60 AERONET sites prior to the C6 reprocessing, Sayer *et al.* [2013] found that the EE could be modeled as

$$EE = \frac{a + b\tau_M}{1/\mu_0 + 1/\mu} \quad (3)$$

where a, b are empirical coefficients, τ_M represents the MODIS AOD, and $1/\mu_0 + 1/\mu$, the sum of reciprocal cosines of the solar and view zenith angles, is the geometric air mass factor (AMF). The AOD-dependence results from the increased sensitivity to assumed aerosol optical properties at high AOD, while the geometric dependence results because larger AMF tends to lead to a larger atmospheric contribution to the TOA signal (decreasing the importance of assumed surface reflectance) while a geometry with smaller AMF tends to be closer to surface reflectance hotspots (increasing the importance of assumed surface reflectance).

This EE expression is a prognostic rather than diagnostic error estimate, as it is defined relative to the retrieved AOD (τ_M) rather than the reference AOD (τ_A). This is because during routine processing, only τ_M is known. Sayer *et al.* [2013] found that for MODIS Aqua, this formulation captured the distribution of AOD retrieval errors well, including dependence on AOD and solar/viewing geometry, and provided a better description of the AOD retrieval error than just the variance of global-average data.

For Aqua data with QA=3 Sayer *et al.* [2013] found $a = 0.086$, $b = 0.56$, such that for a typical $AMF \approx 2.8$, $EE = \pm(0.03 + 0.2\tau_M)$. The same analysis was performed prior to the Terra C6 reprocessing with the same 60 AERONET sites; the derived coefficients are given in Table 1. For Terra data with QA = 3 and $AMF = 2.8$, $EE = \pm(0.03 + 0.23\tau_M)$, slightly larger than Aqua uncertainties. This is expected given the larger calibration uncertainties, even after corrections, on MODIS Terra than Aqua.

Diagnostic (relative to τ_A) uncertainty estimates are also often presented in satellite AOD validation studies as a way to identify errors with respect to a ground truth [e.g., Kahn *et al.*, 2010; Bréon *et al.*, 2011; Sayer *et al.*, 2014, among others]. For DB, the formulation $EE_D = \pm(0.05 + 0.2\tau_A)$ has been used [e.g., Sayer *et al.*, 2012a; Hsu *et al.*, 2013], where the subscripted D here indicates it is a diagnostic rather than prognostic error estimate. Prognostic EE may be more useful when confronted with an individual case study or for applications such as data assimilation [e.g., Zhang and Reid, 2006], but EE_D is more useful when comparing different data sets because it is relative to the same baseline and independent of the retrievals in question [e.g., Bréon *et al.*, 2011, 2006; Sayer *et al.*, 2014], although in this instance performance exceeds the notional 68% compliance implied

Table 1. Prognostic Expected Error (EE) Confidence Envelopes for MODIS Terra C6 Deep Blue Retrievals

QA Value	Expression	For $1/\mu_0 + 1/\mu \approx 2.8$
3	$(0.077 + 0.65\tau_M)/(1/\mu_0 + 1/\mu)$	$0.03 + 0.23\tau_M$
2	$(0.12 + 0.58\tau_M)/(1/\mu_0 + 1/\mu)$	$0.04 + 0.21\tau_M$
1	$(0.079 + 0.94\tau_M)/(1/\mu_0 + 1/\mu)$	$0.03 + 0.34\tau_M$

Table 2. Statistics of DB/AERONET Comparison for Vegetated Sites (Figure 4)^a

Site Name	Latitude (°)	Longitude (°)	Number of Matchups	<i>R</i>			RMS Error			f_{EE}			f_{EED}		
				C5	C6-	C6	C5	C6-	C6	C5	C6-	C6	C5	C6-	C6
Alta Floresta	−9.87100	−56.1040	1111	0.97	0.97	0.97	0.107	0.103	0.104	0.84	0.87	0.89	0.90	0.91	0.91
Bondville	40.0530	−88.3720	1203	0.85	0.83	0.83	0.0721	0.0753	0.0745	0.72	0.73	0.74	0.84	0.82	0.83
Buenos Aires	−34.5670	−58.5000	1265	0.69	0.64	0.64	0.0588	0.0684	0.0664	0.72	0.66	0.68	0.80	0.74	0.77
GSFC	38.9920	−76.8400	1703	0.91	0.91	0.91	0.0662	0.0703	0.0674	0.79	0.73	0.77	0.86	0.80	0.83
Lille	50.6120	3.14200	851	0.81	0.86	0.86	0.0840	0.0702	0.0704	0.65	0.77	0.75	0.75	0.82	0.84
Moldova	47.0000	28.8160	1494	0.86	0.91	0.91	0.0719	0.0561	0.0565	0.70	0.85	0.85	0.82	0.92	0.91
Overall			7627	0.93	0.93	0.93	0.0765	0.0740	0.0733	0.74	0.77	0.78	0.83	0.84	0.85

^a*R* indicates Pearson's linear correlation coefficient, RMS the root-mean-square error, f_{EE} the fraction agreeing within prognostic EE (equation (3)), and f_{EED} the fraction agreeing within the diagnostic EE metric (0.05 + 0.2 τ_A).

by this metric. Thus, both metrics are used at different points here. Note that although the actual retrieval error budget is not modeled perfectly by these types of EE expressions [e.g., Sayer *et al.*, 2013, 2014], as other factors may also be important and as the focus of this study is the comparative effect of different L1b data on the same subset of retrievals, this is of secondary importance in the present case.

3.3. Comparison Results

Tables 2 and 3 provide statistics of comparison results on a site-by-site basis and in aggregate for the vegetated and arid sites respectively. A few general remarks can be made. Applying all calibration updates (the C6 run) improves the statistics of the comparison in aggregate, although individual sites can experience either an enhancement or degradation of performance. Those cases where performance gets slightly worse going from C5 to C6- to C6 L1bs (e.g., Buenos Aires) likely correspond to cases where a compensating bias in the algorithm (such as associated with surface reflectance or aerosol optical model selection) at a particular location was counteracted by a bias in the older L1b calibration data. However, for these cases any decrease of performance quality tends to be small, while the overall picture is one of more significant improvement. The arid sites (Table 3) also tend to show a larger improvement than the vegetated sites (Table 2), which is expected because in general the largest calibration changes are made in band 8 [Jeong *et al.*, 2011; Meister *et al.*, 2014], which is used only by the arid DB processing path. Finally, performance tends to be better overall at vegetated

Table 3. As Table 2, Except for the 16 Arid Sites in Figure 4

Site name	Latitude (°)	Longitude (°)	Number of Matchups	<i>R</i>			RMS Error			f_{EE}			f_{EED}		
				C5	C6-	C6	C5	C6-	C6	C5	C6-	C6	C5	C6-	C6
Banizoumbou	13.5410	2.66500	1985	0.87	0.91	0.91	0.226	0.178	0.179	0.52	0.66	0.68	0.56	0.67	0.72
Beijing	39.9770	116.381	2016	0.91	0.92	0.93	0.228	0.208	0.194	0.56	0.61	0.67	0.66	0.70	0.76
Birdsville	−25.8990	139.346	1510	0.35	0.34	0.33	0.0700	0.0726	0.0703	0.69	0.60	0.67	0.78	0.69	0.77
Dakar	14.3940	−16.9590	1242	0.75	0.80	0.80	0.299	0.235	0.230	0.20	0.32	0.34	0.24	0.37	0.38
Evora	38.5680	−7.91200	1917	0.48	0.53	0.56	0.105	0.0978	0.0944	0.64	0.72	0.76	0.81	0.86	0.90
Fresno	36.7820	−119.773	2218	0.74	0.74	0.74	0.0635	0.0649	0.0640	0.71	0.76	0.78	0.84	0.84	0.84
IER Cinzana	13.2780	−5.93400	1842	0.85	0.88	0.88	0.199	0.177	0.178	0.57	0.64	0.65	0.62	0.66	0.66
Ispra	45.8030	8.62700	1711	0.90	0.92	0.92	0.0970	0.0892	0.0903	0.59	0.67	0.66	0.77	0.84	0.84
Kanpur	26.5130	80.2320	1541	0.81	0.85	0.85	0.219	0.187	0.185	0.67	0.78	0.78	0.68	0.78	0.79
Mongu	−15.2540	23.1510	1604	0.94	0.93	0.94	0.0713	0.0751	0.0739	0.85	0.84	0.86	0.89	0.87	0.88
Saada	31.6260	−8.15600	1804	0.31	0.26	0.35	0.188	0.187	0.185	0.40	0.37	0.42	0.52	0.49	0.55
Sede Boker	30.8550	34.7820	3122	0.42	0.49	0.49	0.167	0.190	0.179	0.34	0.22	0.28	0.34	0.22	0.28
Sevilleta	34.3550	−106.885	1855	0.56	0.56	0.60	0.0549	0.0517	0.0520	0.70	0.71	0.72	0.89	0.90	0.90
Skukuza	−24.9920	31.5870	1091	0.86	0.86	0.86	0.0711	0.0694	0.0707	0.70	0.76	0.72	0.89	0.91	0.90
Solar Village	24.9070	46.3970	2733	0.69	0.76	0.76	0.182	0.160	0.160	0.51	0.61	0.60	0.55	0.62	0.63
Tinga Tingana	−28.9760	139.991	1012	0.46	0.52	0.52	0.0607	0.0623	0.0617	0.71	0.71	0.75	0.82	0.82	0.85
Overall			29203	0.85	0.87	0.88	0.164	0.149	0.145	0.57	0.61	0.63	0.66	0.68	0.70

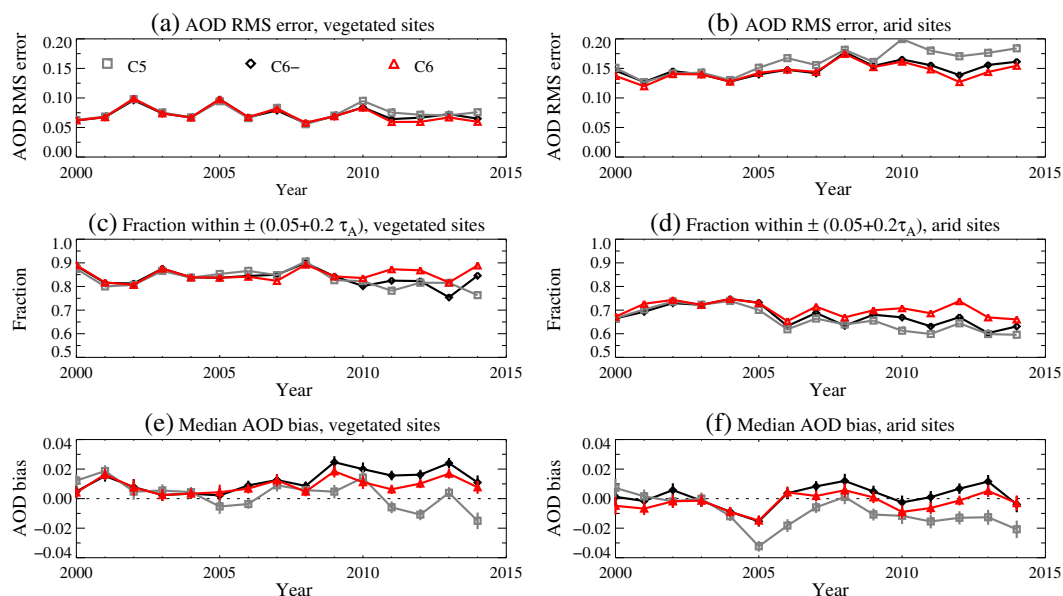


Figure 6. Time series of AERONET validation statistics for (left) vegetated and (right) arid sites. (a and b) The root mean square (RMS) error, (c and d) the fraction in agreement with AERONET within $\pm EE_D$, and (e and f) the median (MODIS-AERONET) AOD bias. Error bars in Figures 6e and 6f indicate the standard error on the median. Gray squares indicate the C5 calibration run, black diamonds the C6- run, and red triangles the C6 run.

than arid sites, due to the former's generally lower AOD (and so less sensitivity to aerosol optical property assumptions) and also lower uncertainties related to surface reflectance modeling and cloud screening over these darker surfaces.

As sensor degradation and calibration corrections are a function of time, it is worthwhile to examine the temporal dependence of validation statistics. Figure 6 shows a time series of comparison statistics aggregated for the two types of sites considered. In general, the C6 data show the greatest stability through the time series and the highest quality of calibration statistic (i.e., lowest RMS error, highest fraction matching AERONET within $\pm EE_D$, bias nearest to zero). Interannual variability is related both to changes in calibration as well as changes in the underlying AOD fields sampled at the AERONET sites. As before, smaller errors are found for vegetated sites than arid sites, and arid sites show a larger difference in comparison quality between calibration versions, with a divergence first becoming apparent around 2005. Caution is advised in interpreting results for 2014 because of the lower data volume in this year (Figure 5), although 2014 results appear to be similar to other recent years (2010–2013).

This is an important result because it shows that the MSCT and OBPB radiometric calibration updates, which are independent of the DB algorithm and of the AERONET validation data, result in a quantifiable improvement of the retrieved AOD. The results illustrate the importance of ongoing monitoring of radiometric calibration, to ensure a stable data record.

For vegetated sites, in recent years (2010 onward) the improvement in RMS error is generally small (<0.02) and the main improvement seems to be related to the stability of the AOD retrieval bias (C5 shows a downward trend and C6- an upward, while C6 has a more consistent small median positive bias). This corresponds to $\sim 5\%$ more points matching AERONET within $\pm EE_D$.

The improvements in RMS error and fraction within $\pm EE_D$ are about twice as large for arid sites. For the more recent years, switching from C5 to C6- calibration decreases RMS by 0.03, and applying the additional OBPB calibration corrections (C6 run) yields a further decrease of 0.01, resulting in a total decrease of aggregated RMS error from ~ 0.18 to ~ 0.14 . The two calibration updates (C5 to C6- and C6- to C6) also each provide incremental increases of ~ 0.05 to the fraction matching AERONET within $\pm EE_D$. In contrast to the vegetated sites,

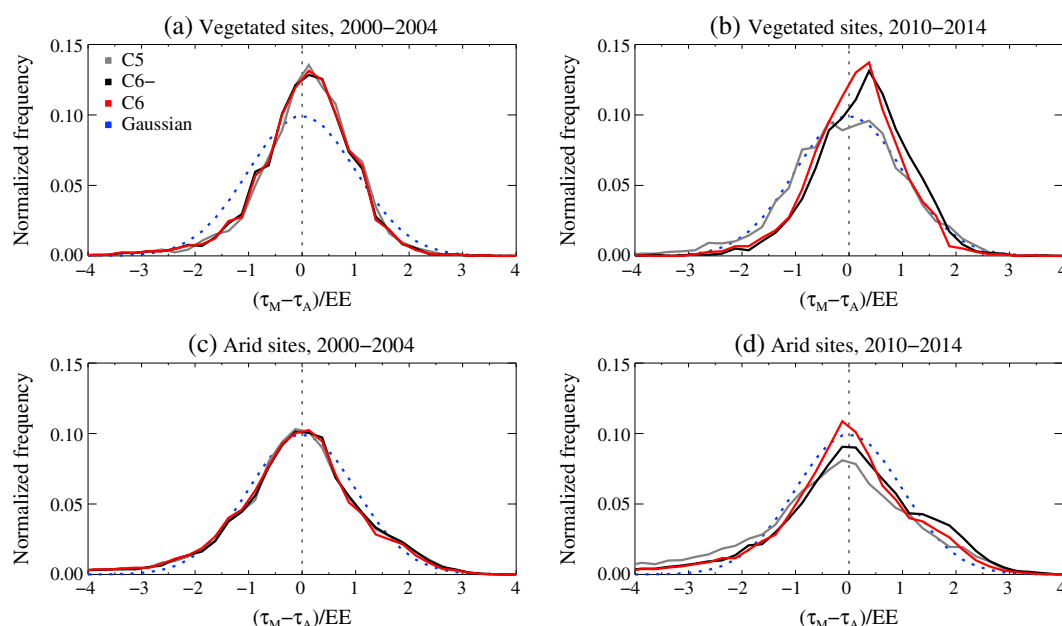


Figure 7. Histograms of AOD retrieval error relative to expected error, for (a and b) vegetated and (c and d) arid sites, for (Figures 7a and 7c) the first and (Figures 7b and 7d) the most recent 5 years of the Terra mission. Data shown for the three calibration runs as well as (in blue) a Gaussian distribution.

without these calibration updates, in recent years the comparison statistics tend to degrade outside the range of variability in earlier years. This supports the decision made during C5 processing to halt production at the end of 2007 [Jeong *et al.*, 2011] but also illustrates that at present, calibration corrections are of a sufficiently high quality that C6 production can continue throughout the whole Terra time series to date. The changes in bias, if calibration had remained uncorrected, had the potential to alias into false trending in derived data products; indeed, this trending had been observed in some C5 data products from MODIS Terra [e.g., Levy *et al.*, 2010; Lyapustin *et al.*, 2014].

The contrast between earlier and later mission data quality is highly evident in Figure 7, which shows histograms of the AOD retrieval error normalized by the expected error (i.e., $[\tau_M - \tau_A]/EE$, cf. Table 1). For the period 2000–2004, histograms for all three calibration runs align closely with one another, while for the period 2010–2014, histograms for the C6 run remain similar while those for the C5 and C6- runs become increasingly skewed and/or broad. Thus, the EE data provided within the operational C6 products are likely to be equally appropriate throughout the Terra mission to date. As noted earlier, the EE formulations are designed so that these histograms should approximate Gaussians with mean of 0 and variance 1; while this appears reasonable for arid sites (using the C6 calibration run), the histograms are narrower than expected for vegetated sites, suggesting scope for further refinement of this formulation [Sayer *et al.*, 2013] in future data versions.

Sayer *et al.* [2013] also presented a comparison of validation statistics between DB data from C5 and C6 for MODIS Aqua for selected (mainly bright-surface) AERONET sites. In that case, the majority of the difference between the two versions was due to DB algorithm updates rather than radiometric calibration updates. Although the change in performance between C5 and C6 depended on the site in question, the C6 data overall provided improved comparative statistics against AERONET: the total number of points with QA = 2 or QA = 3 increased slightly, but the fraction of points in agreement with AERONET by various EE metrics increased by typically of order ~ 0.1 across the whole mission (but by up to 0.6 at some sites). By comparison with Figure 6, this suggests that the relative importance of calibration updates compared to retrieval algorithm updates is small early in the mission but that they are more comparable in magnitude in more recent years, further supporting the need for continual evaluation and refinement of MODIS' radiometric calibration.

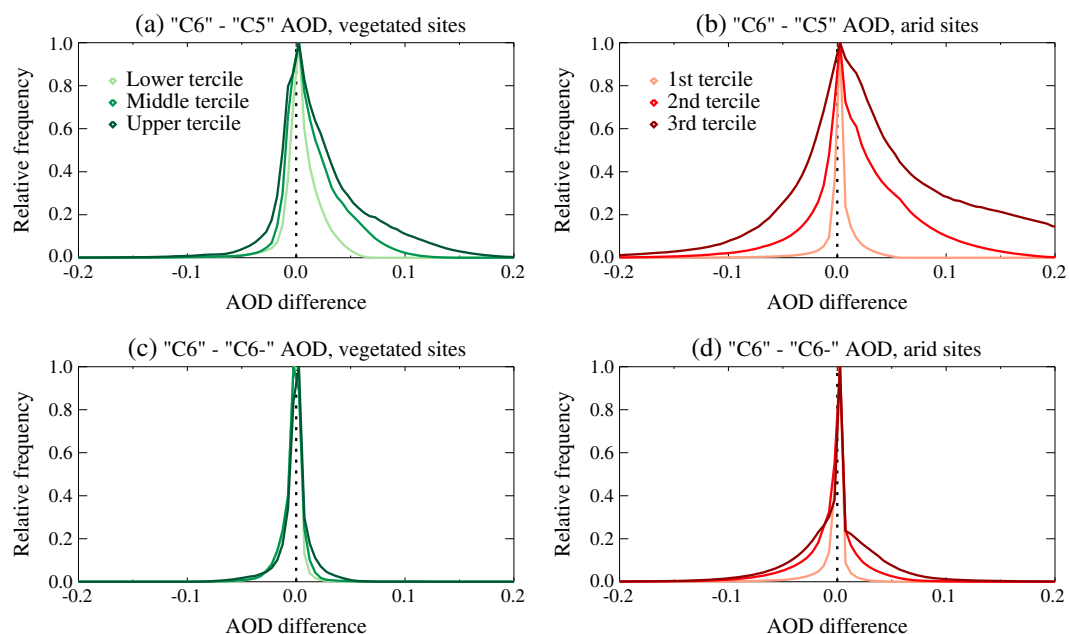


Figure 8. Differences in L2 AOD between the C6 and (a, b) C5 or (c, d) C6- calibration runs, for (a, c) vegetated and (b, d) arid sites. Histograms are split by terciles of AOD from the C6 run. Note that the histograms are truncated at ± 0.2 here, although differences may be larger.

3.4. Distributions of MODIS AOD

As well as retrieval validation against AERONET, it is worthwhile to examine how the distribution of retrieved AOD is affected by the changes in radiometric calibration; for example, how the peak and spread of the distributions change. Using all L2 data from granules overpassing the vegetated AERONET sites, the median, mean, and standard deviation of AOD for the C6 run are 0.12, 0.17, and 0.18, respectively. For the arid sites, these values are 0.13, 0.23, and 0.30. The higher mean than median AOD results from a long high-AOD tail on the distributions, as AOD distributions are close to lognormal [e.g., O'Neill *et al.*, 2000]. For the C5 and C6- runs the standard deviations are stable to within 0.005 of these values, but the means and medians decrease by up to 0.02 for the C5 run and increase by around 0.01 for the C6- run. This indicates that the primary effect of the calibration changes on the AOD distributions is a shift, rather than a change in the width of the distribution.

Figure 8 shows histograms of the difference between the AOD from the C6 run and the C5/C6- runs, stratified by terciles of the C6 AOD. The breakpoints of these AOD terciles are 0.083 and 0.172 for the vegetated sites and 0.071 and 0.240 for the arid sites. The distributions are close to Gaussian (albeit more peaked) for the lower terciles. This is consistent with the response of TOA reflectance to changes in AOD often being close to linear when the AOD is low (i.e., a small perturbation to calibration translates near linearly to a small change in AOD). For the middle and upper AOD terciles, the distributions become broader and increasingly skewed (positive for the C5 comparison and negative for the C6- comparison). The signs of the skew are consistent with Figure 6, and the broadness results from the fact that as AOD increases, the linearity in its relationship with TOA reflectance breaks down, leading to a larger change in retrieved AOD for the same scaling to reflectance. The distributions are also broader for arid sites compared to vegetated sites, due to the brighter surface (hence brighter TOA signal) and the fact that both retrieval bands used have an OBPG correction and are broader for the C6/C5 comparison than the C6/C6- comparison consistent with the OBPG corrections being a smaller perturbation on top of the MCST calibration updates from C5 to C6.

Note that these results represent only those MODIS granules passing over the AERONET sites used, so do not provide a true global picture. However, as they encompass a broad variety of surface/atmospheric conditions,

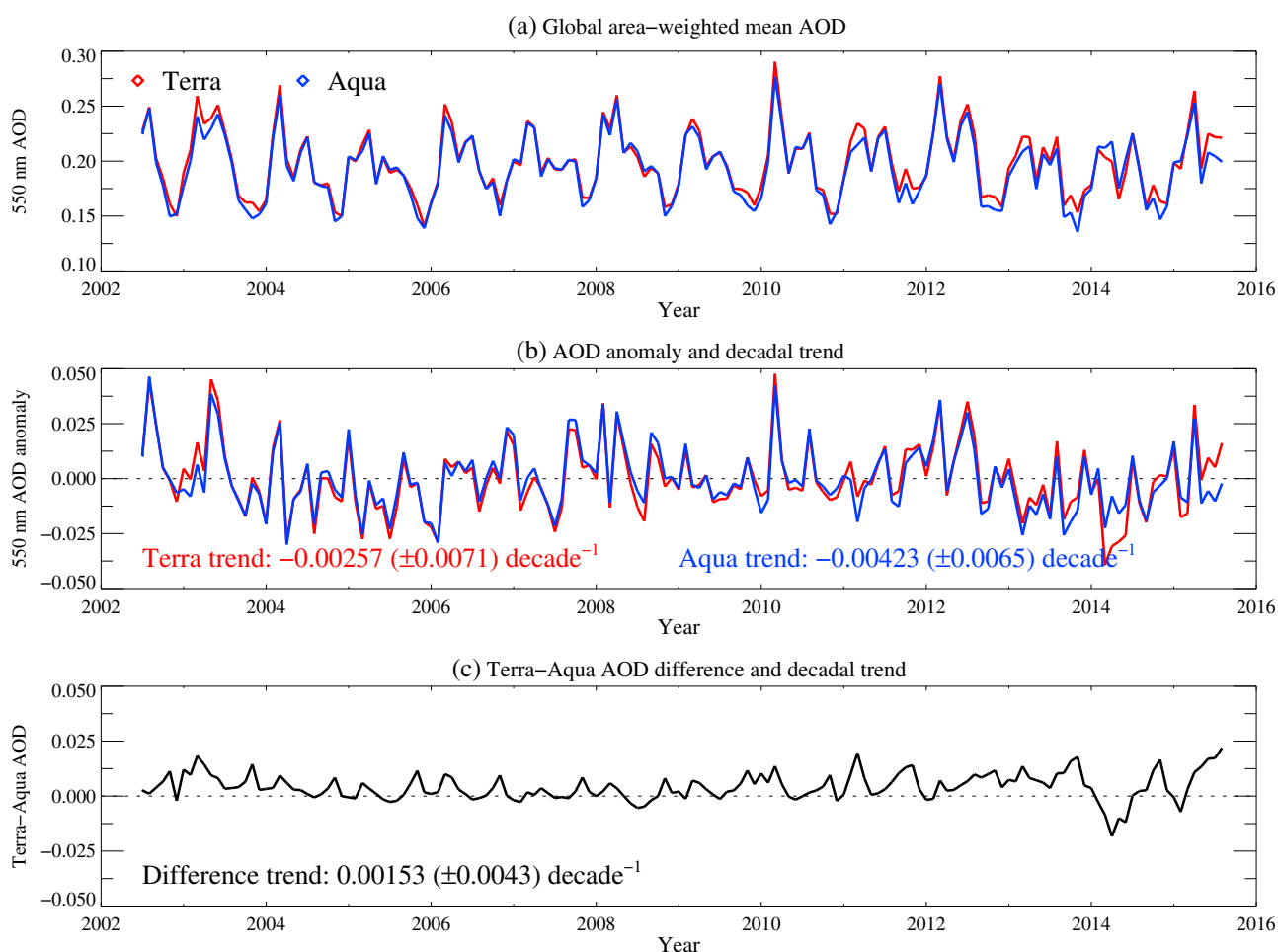


Figure 9. Global over land area-weighted time series of DB (a) AOD at 550 nm and (b) AOD anomaly and decadal trends, from MODIS Terra (red) and Aqua (blue), and (c) the time series and decadal trend in the Terra-Aqua AOD difference. Uncertainties in calculated trends are presented as 90% confidence intervals.

from a representative set of solar/viewing geometries, they are likely to reflect the typical magnitude of AOD distribution changes resulting from calibration changes.

4. Terra-Aqua Consistency

This section uses Level 3 (L3) data to investigate the consistency between global and regional AOD derived from MODIS Terra and Aqua. The daily L3 products provide mean AOD gridded to 1° horizontal resolution from all granules collected on a given calendar date. To minimize the influence of sampling effects from day-to-day coverage differences on calculated regional/global statistics and time series [e.g., Sayer *et al.*, 2010], analyses in this section use only those grid cells where both Terra and Aqua contained at least three valid retrievals on a given day. For the same reason, the monthly analyses shown require at least 3 days with valid retrievals within a month. The results are numerically only weakly sensitive to the exact thresholds used, although stricter thresholds lead to less coverage in regions of high cloudiness such as tropical rainforests.

Figure 9a shows the time series of global area-weighted mean AOD from both sensors. Global time series such as this are not necessarily useful for analyzing long-term variations in AOD, due to the heterogeneity of aerosol sources and sinks, but may help reveal any trends in the data arising from uncharacterized radiometric calibration changes (which would manifest globally). Note that this section only uses the C6 calibration for Terra, as it is impractical to reprocess the whole MODIS record with both the C5 and C6 L1bs in addition. The time series track each other very closely ($R^2 = 0.96$), although Terra has a median offset of 0.003 compared

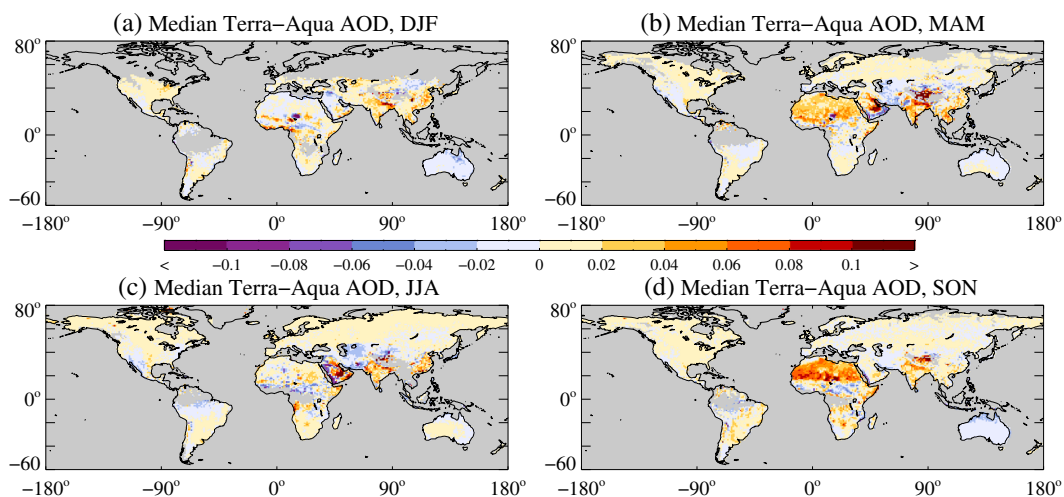


Figure 10. Seasonal median DB Terra-Aqua AOD, calculated from differences in monthly mean data. Grid cells without valid data are shaded in gray.

to Aqua. Figure 9c exhibits some apparent seasonality in the global mean Terra-Aqua AOD offset, which tends to be largest in October/November. Figure 10 shows the seasonal and regional distribution of the offset, for grid cells with at least 5 months contributing to the statistics. The spatiotemporal variability in these maps suggests that calibration differences between the two MODIS instruments cannot explain all the difference. Overall, 59–69% of grid cells (dependent on season) have a median offset smaller than ± 0.01 , and 80–85% smaller than ± 0.02 . Larger offsets tend to be associated with regions of high AOD, e.g., mineral dust, pollution, or biomass burning source regions. Aerosol diurnal variations will also contribute to any offsets; several studies suggest that AOD variations between the Aqua and Terra overpass times are often $\sim 10\%$ relative to the daily average in many regions [Smirnov *et al.*, 2002; Wang *et al.*, 2004; Arola *et al.*, 2013], which is generally consistent with offsets in Figure 10 being < 0.02 for low-AOD areas and larger for high-AOD areas.

It is hard to quantify the individual contributions to this seasonality in the global-average offset. To some extent, it is driven by changes in month-to-month sampling and the underlying AOD fields (e.g., Figure 10), real aerosol diurnal variation, and potentially differences in temporally dependent sensor calibration. Sampling differences within grid cells on a given day may arise from factors such as differences in cloud cover between the two overpass times, which can be nonnegligible [Meskhidze *et al.*, 2009]. Other factors which are likely to contribute include differences in the appropriateness of aerosol scattering phase functions and surface reflectance models at different scattering angles (since the two sensors sample different scattering angles from each other for a particular location and time, and these change throughout the year).

The trend in global mean AOD (Figure 9b), calculated over the common time period using the method of Weatherhead *et al.* [1998], which accounts for autocorrelation in time series when calculating uncertainties

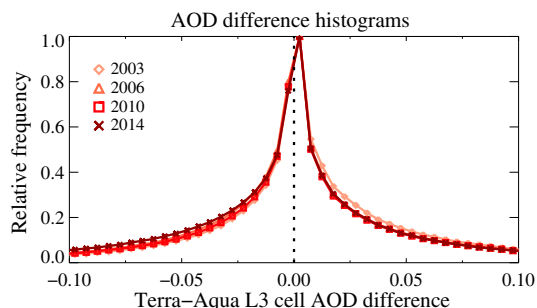


Figure 11. Histograms of Terra-Aqua DB AOD for selected years, from L3 daily data.

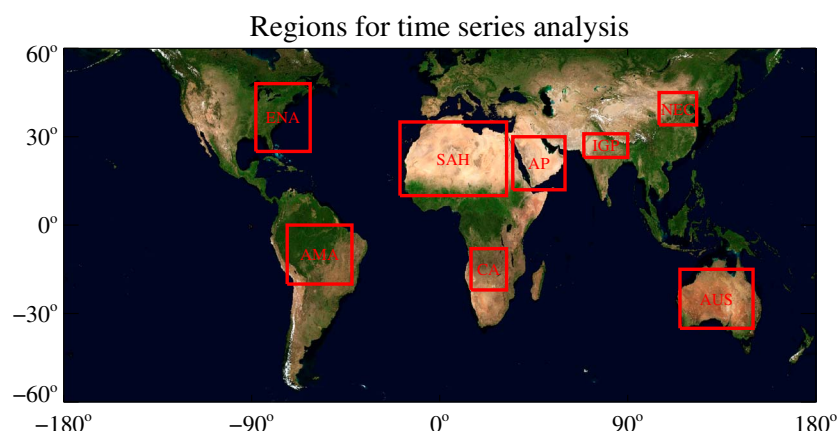
Table 4. Statistics of Terra-Aqua L3 AOD Differences Throughout the Missions

Year	Percentiles of Difference			Mean Difference	Standard Deviation of Difference
	10%	50%	90%		
2003	−0.060	0.003	0.092	0.010	0.109
2006	−0.070	0.000	0.084	0.004	0.112
2010	−0.071	0.001	0.089	0.005	0.117
2014	−0.091	0.000	0.083	−0.003	0.117

and has been used in other aerosol trend studies [e.g., Zhang and Reid, 2010; Hsu et al., 2012], is not significantly different from zero at the 90% level in either sensor. The 90% confidence interval is about ± 0.0065 – 0.0071 decade $^{-1}$. The trend in the Terra-Aqua AOD difference (Figure 9c) is similarly not significantly different from zero (whether calculated as a trend in the AOD difference or, not shown, a trend in the deseasonalized anomaly of the difference) with a similar confidence interval (± 0.0043 decade $^{-1}$). These results imply that the time series are not diverging from each other (within the limits of detectability), suggesting either that the calibration has been characterized sufficiently well to remove detectable artificial trends or else that the two sensors have uncharacterized calibration drifts in the same direction and of similar magnitude, which seems unlikely.

Figure 11 shows histograms of the Terra-Aqua AOD difference calculated from the daily L3 grid cells, as a function of year. Some statistics of these difference histograms are provided in Table 4. These results are broadly consistent with Figure 9, also revealing a slight asymmetry in the difference (mostly, a larger positive than negative tail). There are not large changes in the standard deviation of the difference over time, and the median offset is also stable, although the mean difference shows a slight (order 0.01) shift to less positive values and a broader distribution in 2014 as compared to 2003. However, the data appear to be stable to around the level of AERONET uncertainty (± 0.01) [Eck et al., 1999].

To examine regional variability in the AOD time series, data from eight regions (Figure 12) are shown in Figure 13. The exact choice of regions is somewhat arbitrary, and the examples provided were chosen to encompass a range of different surface conditions (e.g., forested, grass/cropland, suburban, and desert) and aerosol regimes (e.g., mineral dust, biomass burning, industrial, and low continental background). The level of correspondence between the regional time series is similar to or stronger than the global results, with R^2 between 0.94 and 0.996, except for Australia ($R^2 = 0.76$). In this region the typical AOD is low and temporal variability is typically smaller than retrieval uncertainty [Sayer et al., 2013], which is expected to result in a smaller R^2 . The mean offset ranges from -0.006 to 0.014 , also generally consistent with Figures 9–11. It is not straightforward to disentangle to what extent calibration, sampling, and algorithmic assumptions (e.g., quality of assumed magnitude and directional dependence of surface reflectance) contribute to these differences but the results again illustrate that the DB Terra and Aqua records report highly consistent regional, seasonal, and interannual variability without obvious divergence through time.

**Figure 12.** Maps of regions used for Terra/Aqua time series analyses (Figure 13); acronyms defined in Figure 13.

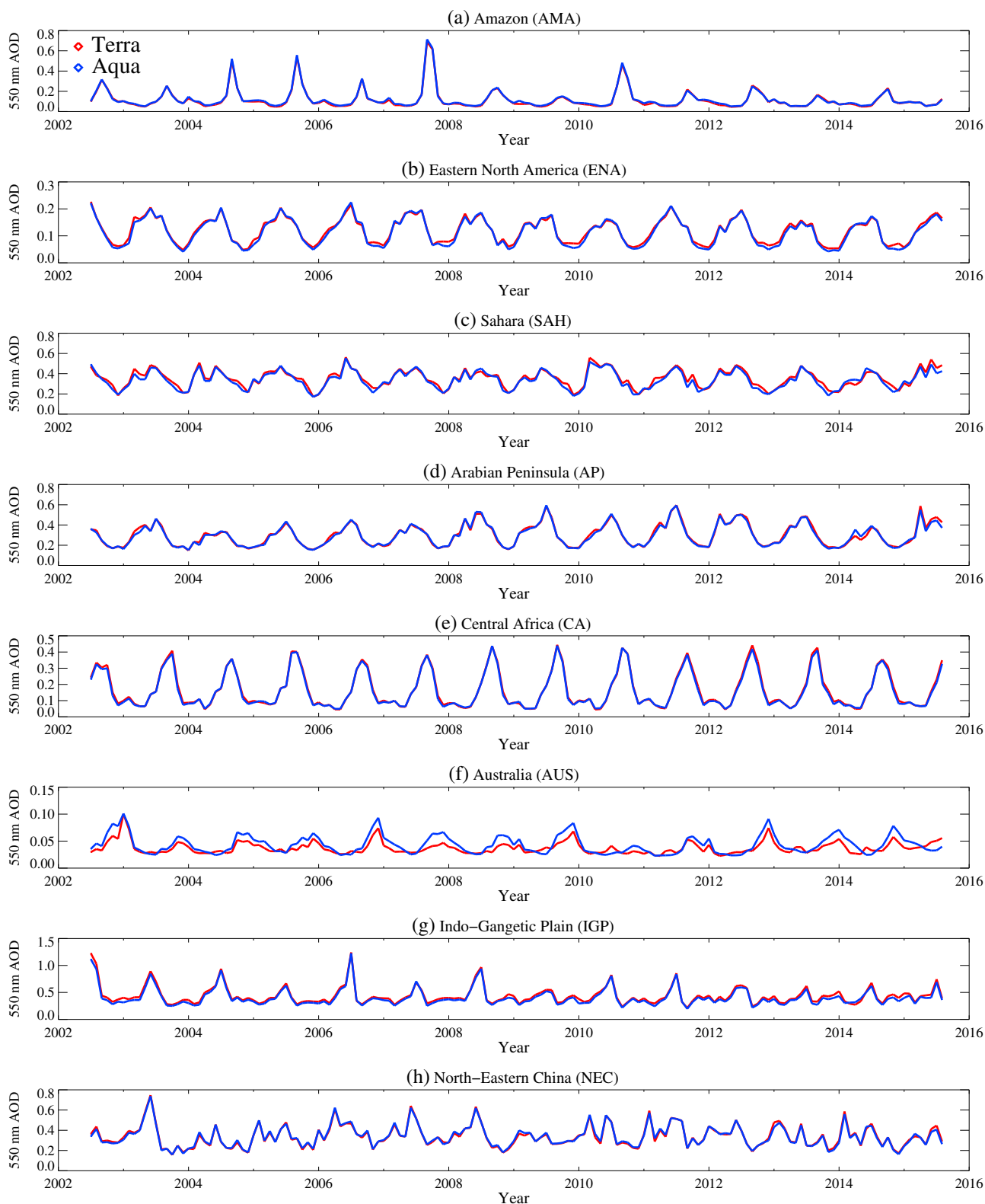


Figure 13. Regional over-land area-weighted time series of DB AOD at 550 nm from MODIS Terra (red) and Aqua (blue) for the regions shown in Figure 12.

5. Conclusions

As well as algorithmic improvements [Hsu *et al.*, 2013], the transition from MODIS C5 to C6 data products involved extensive effort by MCST and OBPB to improve the radiometric calibration of the sensors [Toller *et al.*, 2013; Wu *et al.*, 2013; Meister *et al.*, 2014]. This has been particularly true for MODIS Terra, which has degraded faster than Aqua because it is both older and has had the onboard solar diffuser door open since May 2003, which hampers the onboard calibration [Erives *et al.*, 2004; Franz *et al.*, 2007a].

This study has analyzed the effect of these calibration updates on the C6 Deep Blue aerosol data set and shown that the application of the most recent calibration updates results in the avoidance of a significant deterioration of the quality of retrieved AOD at 550 nm. Specifically, in recent years (~2010 onward), the RMS error compared to AERONET would have increased by ~0.04 over bright surfaces (e.g., deserts, barren soil, and urban areas) and ~0.01–0.02 over darker (e.g., vegetated) land surfaces, and the fraction of points in agreement with AERONET within expected retrieval uncertainty would have degraded by ~10% and ~5%, respectively for these surface types. Given the global average over-land AOD is ~0.2, albeit with large spatiotemporal heterogeneity, this degradation would represent a significant fraction of the typical aerosol loading. Although AOD errors compared to AERONET appear to be slightly larger for Terra than those from MODIS Aqua [Sayer *et al.*, 2013] by around 3% of the AOD, the resulting routinely produced C6 Deep Blue Terra record appears to be temporally stable in terms of comparison against AERONET, and it is expected that this consistent data quality will continue in the coming years.

Comparisons to the Aqua C6 time series reveal a high level of correspondence between the two MODIS DB data records, with a small positive (Terra-Aqua) offset <0.01 globally and in most regions. As the AOD retrieval algorithm applied to the two sensors is the same, this offset represents the aggregate effect of small differences in calibration, diurnally influenced sampling and AOD evolution considerations, and algorithmic uncertainties, and it is nontrivial to quantify how much each factor contributes. However, the stability of this offset throughout the mission and high correspondence of time series ($R^2 = 0.96$ globally, similar or higher in most regions examined) suggests that any uncharacterized radiometric calibration degradation up to the present is either negligible or similar in magnitude and sign between MODIS Terra and Aqua.

Potential future work includes refinement to the expected error (EE) uncertainty metrics contained within the data products [Sayer *et al.*, 2013], as (for both Terra and Aqua) the uncertainties appear to be on aggregate slightly smaller than these estimates over dark (e.g., vegetated) surfaces and slightly larger over bright (e.g., arid) surfaces. This will improve the utility of the data for applications such as data assimilation [Zhang and Reid, 2006; Hyer *et al.*, 2011; Shi *et al.*, 2013] or multisensor data fusion [Chatterjee *et al.*, 2010; Xu *et al.*, 2015], which benefit greatly from quantitative estimation of retrieval uncertainties (as well as, where possible, bias correction). Understanding the situations in which the algorithm does or does not perform well can also lead to ways to improve performance in future data versions and understand discrepancies between different algorithms applied to the same sensor [e.g., Bréon *et al.*, 2011; Sayer *et al.*, 2014].

These results are important because they demonstrate not only the efficacy of the C6 radiometric calibration efforts but also that the C6 MODIS Terra DB AOD data remain stable (to better than 0.01 AOD) and quantitatively similar to Aqua throughout the mission to date. Ongoing efforts will attempt to ensure that this stability is maintained through the future of both missions. This lends confidence to the use of MODIS Terra data for near-real-time and long-term aerosol analyses as a complement to Aqua. With the prior application of DB to SeaWiFS data (1997–2010) [Hsu *et al.*, 2012; Sayer *et al.*, 2012a], and forthcoming release of DB applied to NPP-VIIRS measurements (covering early 2012 onward), this paves the way for an eventual long-term multi-sensor DB data set. The large temporal overlaps between sensors will allow for efficient combination of and bias correction between the sensors, providing a long-term view of the global atmospheric aerosol burden.

References

- Ahmad, Z., B. A. Franz, C. R. McClain, E. J. Kwiatowska, J. Werdell, E. P. Shettle, and B. N. Holben (2010), New aerosol models for the retrieval of aerosol optical thickness and normalized water-leaving radiances from the SeaWiFS and MODIS sensors over coastal regions and open oceans, *Appl. Opt.*, 49(29), 5545–5560, doi:10.1364/AO.49.005545.
- Arola, A., T. F. Eck, J. Huttunen, K. E. J. Lehtinen, A. V. Lindfors, G. Myhre, A. Smirnov, S. N. Tripathi, and H. Yu (2013), Influence of observed diurnal cycles of aerosol optical depth on aerosol direct radiative effect, *Atmos. Chem. Phys.*, 13, 7895–7901, doi:10.5194/acp-13-7895-2013.
- Barnes, W. L., T. S. Pagano, and V. V. Salomonson (1998), Prelaunch characteristics of the Moderate Resolution Imaging Spectroradiometer (MODIS) on EOS-AM1, *IEEE Trans. Geosci. Remote Sens.*, 36(4), 1088–1100, doi:10.1109/36.700993.

Acknowledgments

This work was supported by the NASA EOS program, managed by H. Maring. M.-J. Jeong was supported by the Development of Geostationary Meteorological Satellite Ground Segment program funded by the National Meteorological Satellite Centre of the Korea Meteorological Administration. The authors gratefully acknowledge the AERONET site PIs (C. J. Bruegge, B. Chatenet, H.-B. Chen, P. Goloub, B.N. Holben, A. Karnieli, S. Khabba, C.M.B. Lehmann, D. Moore, B. Mougenot, S. Piketh, A.M. Silva, R. Mitchell, R.P. Singh, D. Tanré, S.N. Tripathi, and G. Zibordi), site managers, supporting institutions, and the AERONET team for the creation and stewardship of the Sun-photometer data records. The MODIS Characterization Support Team and Ocean Biology Processing Group are thanked for their extensive efforts in maintaining the high radiometric quality of MODIS data. AERONET data are available from aeronet.gsfc.nasa.gov and MODIS data from ladsweb.nascom.nasa.gov. Three anonymous reviewers are thanked for their helpful comments on this manuscript.

- Bréon, F. M., A. Vermeulen, and J. Descloitres (2011), An evaluation of satellite aerosol products against sunphotometer measurements, *Remote Sens. Environ.*, **115**(12), 3102–3111, doi:10.1016/j.rse.2011.06.017.
- Chatterjee, A., A. M. Michalak, R. A. Kahn, S. R. Paradise, A. J. Braverman, and C. E. Miller (2010), A geostatistical data fusion technique for merging remote sensing and ground-based observations of aerosol optical thickness, *J. Geophys. Res.*, **115**, D20207, doi:10.1029/2009JD013765.
- Eck, T. F., B. N. Holben, J. S. Reid, O. Dubovik, A. Smirnov, N. T. O'Neill, I. Slutsker, and S. Kinne (1999), Wavelength dependence of the optical depth of biomass burning, urban, and desert dust aerosols, *J. Geophys. Res.*, **104**(D24), 31,333–31,349.
- Erives, H., X. Xiong, J. Sun, J. A. Esposito, S. Xiong, and W. L. Barnes (2004), Terra MODIS RSB on-orbit calibration and performance: Four years of data, *Proc. SPIE 5570, Sensors, Systems, and Next-Generation Satellites VIII*, **5570**, 342–351, doi:10.1117/12.565060.
- Franz, B. A., E. J. Kwiatkowska, G. Meister, and C. R. McClain (2007a), Utility of MODIS-Terra for ocean color applications, *Proc. SPIE 6677, Earth Observing Systems XII*, **6677**, 66770Q, doi:10.1117/12.732082.
- Franz, B. A., S. A. Bailey, P. J. Werdell, and C. R. McClain (2007b), Sensor-independent approach to the vicarious calibration of satellite ocean color radiometry, *Appl. Opt.*, **46**(22), 5068–5082, doi:10.1364/AO.46.005068.
- Gordon, H. R. (1988), Ocean Color remote sensing systems: Radiometric requirements, *Proc. SPIE 0924, Recent Advances in Sensors, Radiometry, and Data Processing for Remote Sensing*, **924**, 151–167, doi:10.1117/12.945683.
- Holben, B. N., et al. (1998), AERONET: A federated instrument network and data archive for aerosol characterization, *Remote Sens. Environ.*, **66**, 1–16, doi:10.1016/S0034-4257(98)00031-5.
- Hsu, N. C., S.-C. Tsay, M. D. King, and J. R. Herman (2004), Aerosol properties over bright-reflecting source regions, *IEEE Trans. Geosci. Remote Sens.*, **42**(3), 557–569, doi:10.1109/TGRS.2004.824067.
- Hsu, N. C., R. Gautam, A. M. Sayer, C. Bettenhausen, C. Li, M. J. Jeong, S.-C. Tsay, and B. N. Holben (2012), Global and regional trends of aerosol optical depth over land and ocean using SeaWiFS measurements from 1997 to 2010, *Atmos. Chem. Phys.*, **12**, 8037–8053, doi:10.5194/acp-12-8037-2012.
- Hsu, N. C., M.-J. Jeong, C. Bettenhausen, A. M. Sayer, R. Hansell, C. S. Sefort, J. Huang, and S.-C. Tsay (2013), Enhanced Deep Blue aerosol retrieval algorithm: The second generation, *J. Geophys. Res. Atmos.*, **118**, 9296–9315, doi:10.1002/jgrd.50712.
- Hyser, E. H., J. S. Reid, and J. Zhang (2011), An over land aerosol optical depth data set for data assimilation by filtering, correction, and aggregation of MODIS Collection 5 optical depth retrievals, *Atmos. Meas. Tech.*, **4**, 379–408, doi:10.5194/amt-4-379-2011.
- Ichoku, C., D. A. Chu, S. Mattoo, Y. J. Kaufman, L. A. Remer, D. Tanré, I. Slutsker, and B. N. Holben (2002), A spatio-temporal approach for global validation and analysis of MODIS aerosol products, *Geophys. Res. Lett.*, **29**(12), doi:10.1029/2001GL013206.
- Jeong, M.-J., N. C. Hsu, E. J. Kwiatkowska, B. A. Franz, G. Meister, and C. E. Salustro (2011), Impacts of cross-platform vicarious calibration on the Deep Blue aerosol retrievals for Moderate Resolution Imaging Spectroradiometer Aboard Terra, *IEEE Trans. Geosci. Remote Sens.*, **49**(12), 4877–4988, doi:10.1109/TGRS.2011.2153205.
- Kahn, R. A., B. J. Gaitley, M. J. Garay, D. J. Diner, T. F. Eck, A. Smirnov, and B. N. Holben (2010), Multiangle Imaging Spectroradiometer global aerosol product assessment by comparison with the Aerosol Robotic Network, *J. Geophys. Res.*, **115**, D23209, doi:10.1029/2010JD014601.
- Kaufman, Y. J., A. E. Wald, L. A. Remer, B.-C. Gao, R.-R. Li, and L. Flynn (1997), The MODIS 2.1 μm channel-correlation with visible reflectance for use in remote sensing of aerosol, *IEEE Trans. Geosci. Remote Sens.*, **35**(5), 1286–1298, doi:10.1109/36.628795.
- Kwiatkowska, E. J., B. A. Franz, G. Meister, C. R. McClain, and X. Xiong (2008), Cross calibration of ocean-color bands from Moderate-Resolution Imaging Spectroradiometer on Terra platform, *Appl. Opt.*, **47**(36), 6796–6810, doi:10.1364/AO.47.006796.
- Levy, R. C., L. A. Remer, R. G. Kleidman, S. Mattoo, C. Ichoku, R. Kahn, and T. F. Eck (2010), Global evaluation of the Collection 5 MODIS dark-target aerosol products over land, *Atmos. Chem. Phys.*, **10**, 10,399–10,420, doi:10.5194/acp-10-10399-2010.
- Levy, R. C., S. Mattoo, L. A. Munchak, L. A. Remer, A. M. Sayer, F. Patadia, and N. C. Hsu (2013), The Collection 6 MODIS aerosol products over land and ocean, *Atmos. Meas. Tech.*, **6**, 2989–3034, doi:10.5194/amt-6-2989-2013.
- Lyapustin, A., Y. Wang, I. Laszlo, R. Kahn, S. Korkin, L. Remer, R. Levy, and J. S. Reid (2011), Multiangle implementation of atmospheric correction (MAIAC): 2. Aerosol algorithm, *J. Geophys. Res.*, **116**, D03211, doi:10.1029/2010JD014986.
- Lyapustin, A., et al. (2014), Scientific impact of MODIS C5 calibration degradation and C6+ improvements, *Atmos. Meas. Tech.*, **7**, 4353–4365, doi:10.5194/amt-7-4353-2014.
- McClain, C. R., G. C. Feldman, and S. B. Hooker (2004), An overview of the SeaWiFS project and strategies for producing a climate research quality global ocean bio-optical time series, *Deep Sea Res.*, **51**, 5–42, doi:10.1016/j.dsr.2.2003.11.001.
- Meister, G., and B. A. Franz (2011), Adjustments to the MODIS Terra radiometric calibration and polarization sensitivity in the 2010 reprocessing, *Proc. SPIE 8153, Earth Observing Systems XVI*, **815308**, doi:10.1117/12.891787.
- Meister, G., E. J. Kwiatkowska, B. A. Franz, F. S. Patt, G. C. Feldman, and C. R. McClain (2005), Moderate-Resolution Imaging Spectroradiometer ocean color polarization correction, *Appl. Opt.*, **44**(26), 5524–5535, doi:10.1364/AO.44.005524.
- Meister, G., B. A. Franz, E. J. Kwiatkowska, and C. R. McClain (2012), Corrections to the calibration of MODIS Aqua ocean color bands derived from SeaWiFS data, *IEEE Trans. Geosci. Remote Sens.*, **50**(1), 310–319, doi:10.1109/TGRS.2011.2160552.
- Meister, G., R. E. Eplee, and B. A. Franz (2014), Corrections to MODIS Terra calibration and polarization trending derived from ocean color products, *Proc. SPIE 9218, Earth Observing Systems XIX*, **9218V**, doi:10.1117/12.2062714.
- Meskhidze, N., L. A. Remer, S. Platnick, R. Negrón Juárez, A. M. Lichtenberger, and A. R. Aiyyer (2009), Exploring the differences in cloud properties observed by the Terra and Aqua MODIS sensors, *Atmos. Chem. Phys.*, **9**, 3461–3475, doi:10.5194/acp-9-3461-2009.
- Munchak, L. A., R. C. Levy, S. Mattoo, L. A. Remer, B. N. Holben, J. S. Schafer, C. A. Hostetler, and R. A. Ferrare (2013), MODIS 3 km aerosol product: Applications over land in an urban/suburban region, *Atmos. Meas. Tech.*, **6**, 1747–1759, doi:10.5194/amt-6-1747-2013.
- O'Neill, N. T., A. Ignatov, B. N. Holben, and T. F. Eck (2000), The lognormal distribution as a reference for reporting aerosol optical depth statistics: Empirical tests using multi-year, multi-site AERONET Sunphotometer data, *Geophys. Res. Lett.*, **27**(20), 3333–3336, doi:10.1029/2000GL011581.
- Remer, L. A., S. Mattoo, R. C. Levy, and L. A. Munchak (2013), MODIS 3 km aerosol product: Algorithm and global perspective, *Atmos. Meas. Tech.*, **6**, 1829–1844, doi:10.5194/amt-6-1829-2013.
- Sayer, A. M., G. E. Thomas, P. I. Palmer, and R. G. Grainger (2010), Some implications of sampling choices on comparisons between satellite and model aerosol optical depth fields, *Atmos. Chem. Phys.*, **10**, 10,705–10,716, doi:10.5194/acp-10-10705-2010.
- Sayer, A. M., N. C. Hsu, C. Bettenhausen, M.-J. Jeong, B. N. Holben, and J. Zhang (2012a), Global and regional evaluation of over land spectral aerosol optical depth retrievals from SeaWiFS, *Atmos. Meas. Tech.*, **5**, 1761–1778, doi:10.5194/amt-5-1761-2012.
- Sayer, A. M., N. C. Hsu, C. Bettenhausen, Z. Ahmad, B. N. Holben, A. Smirnov, G. E. Thomas, and J. Zhang (2012b), SeaWiFS Ocean Aerosol Retrieval (SOAR): Algorithm, validation, and comparison with other data sets, *J. Geophys. Res.*, **117**, D03206, doi:10.1029/2011JD016599.
- Sayer, A. M., N. C. Hsu, C. Bettenhausen, and M.-J. Jeong (2013), Validation and uncertainty estimates for MODIS Collection 6 “Deep Blue” aerosol data, *J. Geophys. Res.*, **118**, 7864–7872, doi:10.1002/jgrd.50600.

- Sayer, A. M., L. A. Munchak, N. C. Hsu, R. C. Levy, C. Bettenhausen, and M.-J. Jeong (2014), MODIS Collection 6 aerosol products: Comparison between Aqua's e-Deep Blue, Dark Target, and merged data sets, and usage recommendations, *J. Geophys. Res.*, *119*, 13,965–13,989, doi:10.1002/2014JD022453.
- Shi, Y., J. Zhang, J. S. Reid, E. J. Hyer, and N. C. Hsu (2013), Critical evaluation of the MODIS Deep Blue aerosol optical depth product for data assimilation over North Africa, *Atmos. Meas. Tech.*, *6*, 949–969, doi:10.5194/amt-6-949-2013.
- Smirnov, A., B. N. Holben, T. F. Eck, O. Dubovik, and I. Slutsker (2000), Cloud-screening and quality control algorithms for the AERONET database, *Remote Sens. Environ.*, *73*(3), 337–349.
- Smirnov, A., B. N. Holben, T. F. Eck, I. Slutsker, B. Chatenet, and R. T. Pinker (2002), Diurnal variability of aerosol optical depth observed at AERONET (Aerosol Robotic Network) sites, *Geophys. Res. Lett.*, *29*(23), doi:10.1029/2002GL016305.
- Sorek-Hamer, M., I. Kloog, P. Koutrakis, A. W. Strawa, R. Chatfield, A. Cohen, W. L. Ridgway, and D. M. Broday (2015), Assessment of PM_{2.5} concentrations over bright surfaces using MODIS satellite observations, *Remote Sens. Environ.*, *163*, 180–185, doi:10.1016/j.rse.2015.03.014.
- Sun, J., X. Xiong, W. Barnes, and B. Guenther (2007), MODIS reflective solar bands on-orbit Lunar calibration, *IEEE Trans. Geosci. Remote Sens.*, *45*(7), 2383–2393, doi:10.1109/TGRS.2007.896541.
- Sun, J.-Q., and X. Xiong (2007), MODIS polarization-sensitivity analysis, *IEEE Trans. Geosci. Remote Sens.*, *45*(9), 2875–2885, doi:10.1109/TGRS.2007.900672.
- Toller, G., X. Xiaoxiong, J. Sun, B. N. Wenny, X. Geng, J. Kuyper, A. Angal, H. Chen, S. Madhavan, and A. Wu (2013), Terra and Aqua Moderate-Resolution Imaging Spectroradiometer collection 6 level 1b algorithm, *J. Appl. Remote Sens.*, *7*(1), 073557, doi:10.1117/1.JRS.7.073557.
- Wang, J., X. Xia, P. Wang, and S. A. Christopher (2004), Diurnal variability of dust aerosol optical thickness and Angström exponent over dust source regions in china, *Geophys. Res. Lett.*, *31*, L08107, doi:10.1029/2004GL019580.
- Weatherhead, E. C., G. C. Reinsel, G. C. Tiao, X.-L. Meng, D. Choi, W.-K. Cheang, T. Keller, J. DeLuise, D. J. Wuebbles, J. B. Kerr, A. J. Miller, S. J. Oltmans, and J. E. Frederick (1998), Factors affecting the detection of trends: Statistical considerations and applications to environmental data, *J. Geophys. Res.*, *103*(D14), 17,149–17,161, doi:10.1029/98JD00995.
- Wu, A. S., X. X. Xiong, D. R. Doelling, D. Morstad, A. Angal, and R. Bhatt (2013), Characterization of Terra and Aqua MODIS VIS, NIR, and SWIR spectral bands' calibration stability, *IEEE Trans. Geosci. Remote Sens.*, *51*(7), 4330–4338, doi:10.1109/TGRS.2012.2226588.
- Xiong, X., J. Sun, W. Barnes, V. Salomonson, J. Esposito, H. Erives, and B. Guenther (2007), Multiyear on-orbit calibration and performance of Terra MODIS reflective solar bands, *IEEE Trans. Geosci. Remote Sens.*, *45*(4), 879–889, doi:10.1109/TGRS.2006.890567.
- Xu, H., J. Guang, Y. Xue, G. de Leeuw, Y. H. Che, J. Guo, X. W. He, and T. K. Wang (2015), A consistent aerosol optical depth (AOD) dataset over mainland China by integration of several AOD products, *Atmos. Env.*, *114*, 48–56, doi:10.1016/j.atmosenv.2015.05.023.
- Zhang, J., and J. S. Reid (2006), MODIS aerosol product analysis for data assimilation: Assessment of over-ocean level 2 aerosol optical thickness retrievals, *J. Geophys. Res.*, *111*, D22207, doi:10.1029/2005JD006898.
- Zhang, J., and J. S. Reid (2010), A decadal regional and global trend analysis of the aerosol optical depth using a data-assimilation grade over-water MODIS and Level 2 MISR aerosol products, *Atmos. Chem. Phys.*, *10*, 10,949–10,963, doi:10.5194/acp-10-10949-20109.